Quantitative NDE of pipe wall thinning using pulsed eddy current testing method

東北大学	解　社娟	Shejuan XIE	Member
東北大学	高木　敏行	Toshiyuki TAKAGI	Member
東北大学	内一　哲哉	Tetsuya UCHIMOTO	Member
中国西安交通大学	陳　振茂	Zhenmao CHEN	Member

Abstract: In nuclear power plants (NPPs), due to flow accelerated corrosion (FAC) and liquid droplet impingement (LDI) of the coolant inside the pipe, there may happen local wall thinning defects on the inner surface of a pipe. Concerning the material of pipes, there are mainly two types, low-carbon steel and stainless steel. In this paper, the feasibility of quantitative nondestructive evaluation (QNDE) to wall thinning in stainless steel pipes using pulsed eddy current testing (PECT) method is discussed. Two major works are conducted in this study. The first part work is that an efficient forward numerical simulation solver for PECT signals has been proposed and developed based on the Fourier series method combined with an interpolation strategy and the database approach. The second part work is that an inversion algorithm of PECT has been proposed and validated, based on the developed efficient simulator of PECT signals and a deterministic optimization strategy, for the profile reconstruction of wall thinning in pipes of NPPs. Through the QNDE of pipe wall thinning based on the developed efficient PECT forward simulator and inversion analysis using the experimental PECT signals of simulated specimen, the efficiency and the robustness of the proposed PECT forward and inversion algorithm have been demonstrated, and the feasibility of PECT for wall thinning QNDE is also validated.

Keywords: Pipe wall thinning, Quantitative NDE, Pulsed eddy current testing, Fast forward simulator, Inverse analysis

1 Introduction

In nuclear power plants (NPPs), due to flow accelerated corrosion (FAC) and liquid droplet impingement (LDI) of the coolant inside the pipe, there may happen local wall thinning defects on the inner surface of a pipe [1]. Concerning the material of pipes, there are mainly two types, low-carbon steel and stainless steel where the stainless steel pipes are targeted in this study. To guarantee the safety of NPPs, periodical nondestructive testing (NDT) to the pipes is mandatory. Another important issue is to check whether the wall thinning exceeds the safe tolerance range. This can not only guarantee safety but also save on unnecessary renewal of pipes. This requires a so-called quantitative NDT (QNDT) method. However, the QNDT of pipe wall thinning in NPPs has so far not been well solved.

Pulsed eddy current testing (PECT) method, due to its rich frequency components and applicability of large electric current, shows outstanding features especially for the detection of defect in deep region [2]. Therefore, PECT is considered as a powerful candidate for the QNDT of wall thinning defect in NPPs.

PECT is a typical transient electromagnetic field problem whose efficient forward simulation tool still has not been well solved [3]. For probe optimization and especially for the inverse analysis of PECT problems, a fast and efficient numerical solver is highly required and is crucial to the calculation of numerous forward problems [4]. The huge computational resources needed for these forward simulations are sometimes beyond the capacity of an average computer. Therefore, an efficient and high accuracy simulator for the forward signal prediction of PECT is indispensable for the further development of PECT technology. On the other hand, as introduced above, the defect profile characterization of pipe wall thinning in NPPs from PECT signals has so far not been well solved, thus the inverse analysis of PECT also needs much effort. Inversion analysis scheme reconstructs the size of a defect from the measured signal, which is the reverse method to the forward analysis [5] where the development of the efficient forward simulation tool of PECT could give a good basis for the quantitative wall thinning analysis based on the inversion techniques.

Based on the backgrounds described above, the objective of the present study is to discuss the feasibility of QNDT to pipe wall thinning using PECT method. The works are mainly on the following two aspects: a) to develop an efficient forward numerical tool for the PECT signal prediction; b) to develop an inversion algorithm for PECT method and apply it for the pipe wall thinning reconstruction.

The contents of this paper are arranged as follows: first, an efficient forward numerical simulator for the PECT signal calculation due to volumetric defect is proposed and developed by introducing the database type fast eddy current testing (ECT) simulation scheme to the Fourier-series-based PECT signal simulation method with help of an interpolation strategy. Then, an inverse analysis scheme of PECT is proposed for the sizing of pipe wall thinning in NPPs, based on a deterministic optimization strategy and the developed efficient forward PECT signal simulator. Finally, the reconstruction examples of wall thinning from PECT signals are given to validate the feasibility of PECT for wall thinning QNDT.

2 Efficient forward simulator for PECT signals

In this work, an efficient forward numerical solver for simulation of the PECT signals was developed based on the database approach and the Fourier series method with help of interpolation strategy. At first, the Fourier series method with interpolation strategy was described for the PECT signals

連絡先: 高木敏行、〒980-8577 仙台市青葉区片平2-1-1、東北大学流体科学研究所、
E-mail: takagi@ifs.tohoku.ac.jp

prediction. Second, the fast numerical solver of database approach was upgraded in order to apply it to the ECT problem of volumetric local wall thinning defect. Finally, based on the Fourier series method and the fast simulation scheme for single frequency excitation, an efficient numerical solver was developed and validated for the simulation of PECT signals due to a local wall thinning. Through comparing the numerical results using the present fast solver and a conventional method (i.e. only using Fourier series method for PECT signal calculation), it was verified that the fast solver can predict the PECT signals accurately and over 100 times faster than the conventional one.

2.1 Fourier series method

When applying PECT, the excitation current $\boldsymbol{I}(t)$ is usually introduced as repetitive pulses of square wave which can be considered as a summation of serial harmonic sinusoidal waves represented by Eq. (1) according to the Fourier transformation theory [6],

$$\boldsymbol{I}(t)=\sum_{n=0}^{N}\widetilde{F}_n e^{\mathrm{j}\omega_n t}, \tag{1}$$

where n=0 means the DC (direct current) component, ω_n is the angular frequency of sinusoidal excitation, $\widetilde{F}_n$ is the amplitude coefficient and j is the imaginary unit. Since the PECT problem can be considered as a low frequency linear electro-magnetic problem, its governing equations can be written as follows after finite element method (FEM) discretization,

$$[K]\{A\}+[C]\left\{\frac{\partial A}{\partial t}\right\}=\{M\}\boldsymbol{I}(t), \tag{2}$$

where A is the vector potential, $[K]$, $[C]$ and $\{M\}$ are coefficient matrices of the FEM equations. Because of the linear property of Eq. (2), the response signal due to pulsed excitation in the form of Eq. (1) is also composed of sinusoidal waves of frequencies appearing in the driving current. After formulae deduction, the response magnetic flux density $\boldsymbol{B}$ can be obtained by summating the response signals of each frequency $\boldsymbol{B}_{n0}$ as shown in Eq. (3) (the DC component is neglected as it does not induce eddy current). When each $\boldsymbol{B}_{n0}$ has been calculated, the field signal $\boldsymbol{B}(t)$ can be obtained by using Eq. (3) simply.

$$\{\boldsymbol{B}(t)\}=\sum_{n=1}^{N}\widetilde{F}_n\left(\nabla\times\left\{\widetilde{A}_{n0}\right\}\right)e^{\mathrm{j}\omega_n t}=\sum_{n=1}^{N}\widetilde{F}_n\left\{\widetilde{\boldsymbol{B}}_{n0}\right\}e^{\mathrm{j}\omega_n t} \tag{3}$$

2.2 Interpolation strategy

To simulate PECT signals based on Eq. (3), it is required to know the response signals of the necessary single frequency sinusoidal excitation, which are calculated using a sinusoidal ECT simulation code. If calculating all the signal components necessary in the summation of Eq. (3) using the full FEM code, the huge computational burden will make this method inapplicable.

As the frequency response curve of single frequency ECT problem is smooth, the amplitude of the response signal of a given harmonic frequency can be calculated from the signals of the selected typical frequencies through interpolation. This idea can shorten the simulation time of single frequency ECT problems. The total number of frequencies for signal summation and the number of selected frequencies for interpolation are very important to guarantee the precision of the Fourier series simulation method, which were carefully discussed in reference [7].

2.3 Fast solver of ECT signal simulation for volumetric defects

A fast solver of ECT signal simulation due to non-volumetric defects (i.e. cracks like) has been developed by authors [8, 9]. As the wall thinning is volumetric defect of 3D geometry, the fast solver has to be upgraded in order to be applied to the ECT signal simulation of wall thinning defect. The major difference between crack and wall thinning problem is the dimension of the databases of the unflawed potentials and the way to establish the inverse matrix. The theory of the fast scheme is as follows:

Through subtracting the governing equations with and without defect and conducting Galerkin FEM discretization, the following system of linear equations can be obtained,

$$\begin{bmatrix}\bar{K}_{11} & \bar{K}_{12}\\ \bar{K}_{21} & \bar{K}_{22}\end{bmatrix}\begin{Bmatrix}A_1^f\\ A_2^f\end{Bmatrix}=\begin{bmatrix}\hat{K}_{11} & 0\\ 0 & 0\end{bmatrix}\begin{Bmatrix}A_1^f+A_1^0\\ A_2^f+A_2^0\end{Bmatrix}, \tag{4}$$

where subscripts 1 and 2 denote the areas at the defect and at the other area, while superscripts f and 0 denote the potentials perturbation due to flaw existence and that of the unflawed material. $[\bar{K}]$ is the unflawed global coefficient matrix of FEM equations.

From Eq. (4), we can obtain a smaller system of linear equations for solving the potential perturbation $\{A_1^f\}$,

$$\left[I-H_{11}\hat{K}_{11}\right]\left\{A_1^f\right\}=[H_{11}][\hat{K}_{11}]\left\{A_1^0\right\}, \tag{5}$$

where $[H]$ is the inverse matrix of $[\bar{K}]$.

Since the coefficient matrix $[H]$ and the unflawed potentials $\{A_1^0\}$ are independent of the flaw geometry, they can be calculated a priori and stored as databases. In this way, calculation burden of $\{A_1^f\}$ can be greatly reduced because the number of the nodes related to defect is always much smaller than that of the whole system. In present work, the database region was extended and the 2D shifting symmetry scheme was proposed to establish databases of inverse matrix $[H]$ and the unflawed field $\{A^0\}$ for treating the volumetric wall thinning defect, and the corresponding numerical code is developed.

2.4 Fast solver of pulsed ECT signal simulation for volumetric defects

Based on the Fourier series method and the interpolation strategy and the fast scheme for ECT signal prediction due to volumetric defect, a fast numerical solver for simulation of PECT signals due to local wall thinning defect is developed. The basic procedure of the code is as follows: initially, the sinusoidal ECT response signals of selected frequencies from local wall thinning are calculated using the fast ECT solver described in Section 2.3. Then, the response signal from the pulsed excitation (PECT signal) can be calculated following the Fourier series method. In this way, the transient PECT signals can be obtained within a very short time.

To validate the efficient PECT simulator, an example is investigated where the inspection target of the numerical model is a plate of austenitic stainless steel 316 of length (*Y* direction) 120 mm, width (*X* direction) 120 mm, and thickness (*Z* direction) 10 mm. The defect is set as a cuboid OD wall thinning 12 mm in length, 33 mm in width and 4 mm in depth. The parameters of the excitation coil are: inner diameter, 5 mm; outer diameter, 10 mm; height, 5 mm and total number of turns, 296. The Lift-offs of both the excitation and pickup elements are 0.5 mm. A square wave pulse is applied to the excitation coil as the driving current whose DC component is 1.0 A, the period is 0.01s and the duty cycle is 50%. Figure 1 shows the schematic of the model. The probe is scanned along the length direction of the defect. The magnetic flux density in the vertical direction at the position of the bottom center of the excitation coil is selected as the pickup signal.

Figure 2 shows the numerical comparison results of pulsed signals between the conventional method (i.e. Fourier series method combined with full FEM approach for harmonic sinusoidal ECT signal prediction) and present fast solver (i.e. Fourier series method combined with the database type fast ECT solver for harmonic sinusoidal ECT signal prediction) for the given example, when the probe is just above the center of the wall thinning defect. Figure 3 shows the numerical comparison results of peak values in pulsed signals between the conventional method and the fast solver, when the probe is scanning along the length direction shown in Fig. 1. In addition, in the Fourier series method, the first 450 harmonic components are used for summation and 30 selected harmonic components are used for interpolation. The relative error (difference) of the PECT signal in Fig. 3 between the conventional method and the fast solver is about 2.1%.

Though all of the above results show very good agreement, the conventional method takes about 9 hours to obtain the results in Fig. 3, while the fast solver needs only about 4 minutes, which is more than 100 times faster. The computation is carried out on a personal computer, consisting of an Intel (R) Core (TM) i7 CPU 960 @ 3.2 GHz, Memory 6 GB, OS Fedora 12 and Intel Fortran Compiler 10.1.

Concerning establishing the databases, in this case it takes about 43 hours to build the databases for the unflawed fields and the inverse matrix. Although this time is rather long, it is only necessary to be established once for inverse analysis of the PECT signals of a given inspection target. Once the database is well established, each forward analysis only takes several minutes compared with the almost intolerable several hours for the conventional method. Thus the proposed fast solver for signal prediction of PECT gives a good basis for the inversion problem in PECT technology.

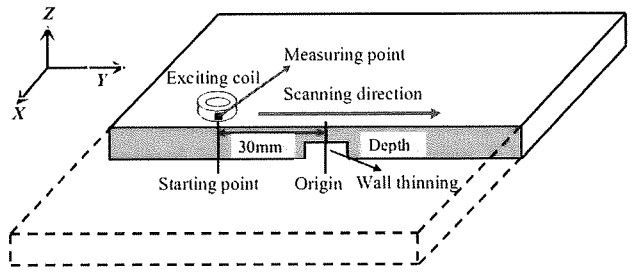

Figure 1. The schematic model for defect detection

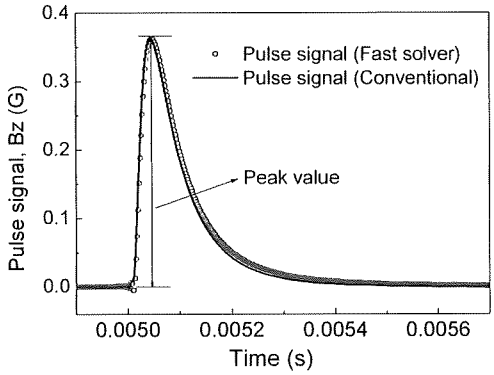

Figure 2. Pulsed signal when probe is above the center of the wall thinning, for comparison of fast solver and conventional method simulation of wall thinning in the considered example under pulsed excitation

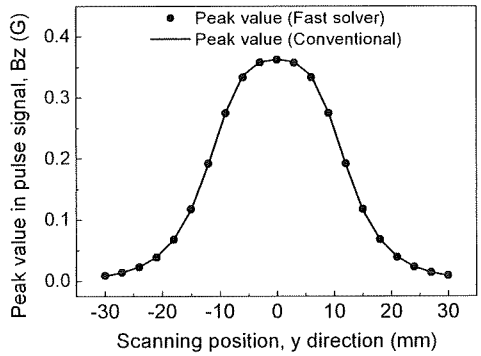

Figure 3. Peak value of pulsed signal when probe is scanning along the length direction, for comparison of fast solver and conventional method simulation of wall thinning in the considered example under pulsed excitation

3 Inversion algorithm of PECT for sizing of wall thinning

In this work, based on the above developed efficient forward PECT signal simulator, a deterministic optimization strategy based reconstruction scheme with the help of Conjugate Gradient (CG) method is proposed and developed to deal with the sizing of local wall thinning in pipes of NPPs.

3.1 Model of wall thinning for reconstruction

As shown in Fig. 4, local wall thinning is modelled as a group of planar slit defects (rows) of given width but of differing length (for example, in the *w*-th row, the length of wall thinning equals *bw–aw*) and depth (in the *w*-th row, the maximum depth of wall thinning to the total thickness of specimen is *dw* (%)). These are selected as the defect shape parameters to be reconstructed. As these parameters have to be simultaneously reconstructed, two-dimensional signals (probe scans along the length and width direction in Fig. 4) scanned over the wall thinning on the far side are used for the reconstruction. In cases where the defect length and depth are close to zero in some rows after reconstruction, then these rows will be treated as an unflawed region. In this way, the width information of the wall thinning can also be properly reconstructed [10].

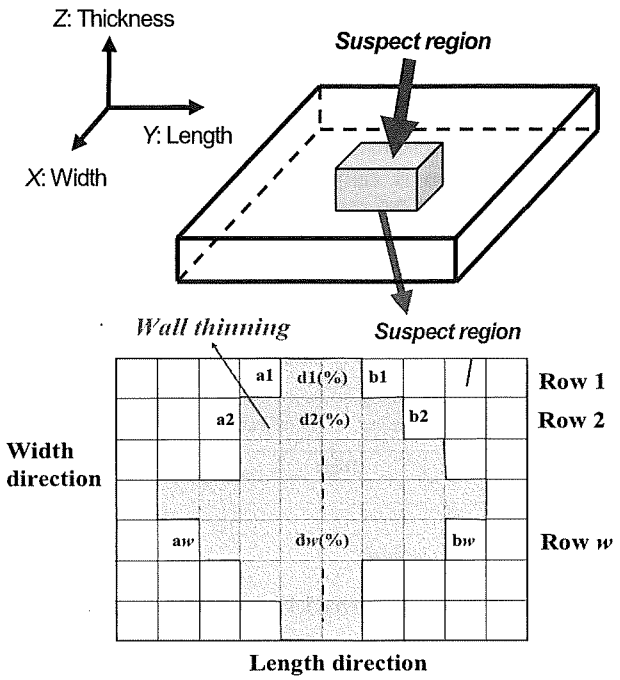

Figure 4. Reconstruction strategy schematic for 3D profile of wall thinning in suspect region

3.2 Principle of inversion algorithm

An inverse analysis method, based on the deterministic optimization algorithm, is used to reconstruct the profile of the 3D wall thinning. This means that the sizing process is converted to an optimization problem of minimizing the objective function,

$$\varepsilon(\boldsymbol{c}^k)=\sum_{l=1}^{L}\sum_{m=1}^{M}\left(P_{l,m}(\boldsymbol{c}^k)-P_{l,m}^{obs}\right)^2 / \sum_{l=1}^{L}\sum_{m=1}^{M}\left(P_{l,m}^{obs}\right)^2, \quad (6)$$

where k is the iteration step, l and m represent the position of 2D scanning point, $\boldsymbol{c}^k$ the shape parameter vector of wall thinning after k-th iteration and $\varepsilon(\boldsymbol{c}^k)$ the objective function (residual error). $P_{l,m}(\boldsymbol{c}^k)$ is the feature parameter extracted from the PECT signal $\boldsymbol{B}(t)$ at (l, m) scanning point for defect shape $\boldsymbol{c}^k$ and $P_{l,m}^{obs}$ is the corresponding feature parameter extracted from the measured signal. In this study, peak value is employed for the feature parameter of the PECT signal, as shown in Eq. (7), where t_0 represents peak time.

$$P(\boldsymbol{r})=B(\boldsymbol{r},t)\big|_{t=t_0} \quad (7)$$

The conjugate gradient (CG) based reconstruction scheme is used to predict the length and depth of the wall thinning in each row. In this study, Eq. (8) is adopted for the direct calculation of the gradient vector from the calculated electric fields for the transmitter-receiver type PECT probe [11].

$$\frac{\partial B(\boldsymbol{r},t)}{\partial c_{w,i}} = -\sigma_0\sum_{n=1}^{N}F_n\left(\alpha\int_S \boldsymbol{E}_p^u\cdot(\boldsymbol{E}_e^u+\boldsymbol{E}_e^f)\frac{\partial s_w(\boldsymbol{c},\boldsymbol{r})}{\partial c_{w,i}}ds\right)e^{j\omega_n t} \quad (8)$$

In Eq. (8), σ_0 is the conductivity of the specimen in unflawed region, $\boldsymbol{E}_p^u$ is the unflawed electric field generated by unit current in the pickup coil, $\boldsymbol{E}_e^u+\boldsymbol{E}_e^f$ is the flawed electric field generated by the excitation coil (including unflawed and perturbed field), α is a coefficient to correspond the output of pickup coil to the PECT signal, $c_{w,i}$ is the i-th wall thinning shape parameter at the w-th planar row in width direction and $s_w(\boldsymbol{c},\boldsymbol{r})=0$ is the equation of the defect boundary surface in w-th row. As for the PECT signal, the feature parameter $\partial P(\boldsymbol{r})/\partial c_{w,i}$ in the signal of the gradient vector is extracted from Eq. (9), where $t=t_0$ (peak time obtained in Eq. (7)), as shown in Eq. (9).

$$\frac{\partial P(\boldsymbol{r})}{\partial c_{w,i}}=\frac{\partial B(\boldsymbol{r},t)}{\partial c_{w,i}}\bigg|_{t=t_0} \quad (9)$$

With the CG based optimization method, the shape parameter vector of wall thinning $\boldsymbol{c}^k$ can be obtained through the following iteration procedure,

$$\boldsymbol{c}^k=\boldsymbol{c}^{k-1}+a^k\times(\delta\boldsymbol{c})^k, \quad (10)$$

where $(\delta\boldsymbol{c})^k$ is the updating direction in the k-th iteration, which is chosen as the direction of the conjugate gradient vector in case of the CG algorithm. This can be obtained using Eq. (11), according to the definition of the CG algorithm.

$$(\delta c_{w,i})^k = \left(\sum_{w,i}\left(\left|\frac{\partial\varepsilon}{\partial c_{w,i}}\right|^2\right)^k / \sum_{w,i}\left(\left|\frac{\partial\varepsilon}{\partial c_{w,i}}\right|^2\right)^{k-1}\right)(\delta c_{w,i})^{k-1} + (\partial\varepsilon/\partial c_{w,i})^k \quad (11)$$

a^k is a step size parameter selected as the value which can reduce $\varepsilon(\boldsymbol{c}^k)$ most efficiently. After formulation it can be obtained as shown in Eqs. (12) and (13).

$$a^k=-\sum_{l=1}^{L}\sum_{m=1}^{M}(P_{l,m}^{\,k-1}-P_{l,m}^{obs})\times\frac{\partial P_{l,m}^{\,k-1}}{\partial a^k} \Big/ \sum_{l=1}^{L}\sum_{m=1}^{M}\left(\frac{\partial P_{l,m}^{\,k-1}}{\partial a^k}\right)^2, \quad (12)$$

$$\frac{\partial P_{l,m}^{\,k-1}}{\partial a^k} = \sum_{w,i}\frac{\partial P_{l,m}^{\,k-1}}{\partial c_{w,i}}\frac{\partial c_{w,i}}{\partial a^k} = \sum_{w,i}\frac{\partial P_{l,m}^{\,k-1}}{\partial c_{w,i}}\left(\frac{\partial\varepsilon}{\partial c_{w,i}}\right)^k \quad (13)$$

Based on the above algorithm, the flowchart of the wall thinning reconstruction procedure is shown in Fig. 5. During

iteration when the residual error is small enough, the computational feature extracted from PECT signals will be very close to the objective feature extracted from the measured PECT signals, which means that the iterative wall thinning shape parameters are near to the real ones. Therefore, the stop conditions are that the residual error is smaller than a certain value ε_c or that the number of iterations is larger than a set value N_c. In the flowchart, the forward simulation part needs to be repeated many times to calculate the PECT signals under different wall thinning parameters. Therefore, the efficient forward simulator is employed here and can significantly reduce the computational burden. According to the flowchart, an inverse analysis code has been developed for the reconstruction of wall thinning from the measured PECT signals.

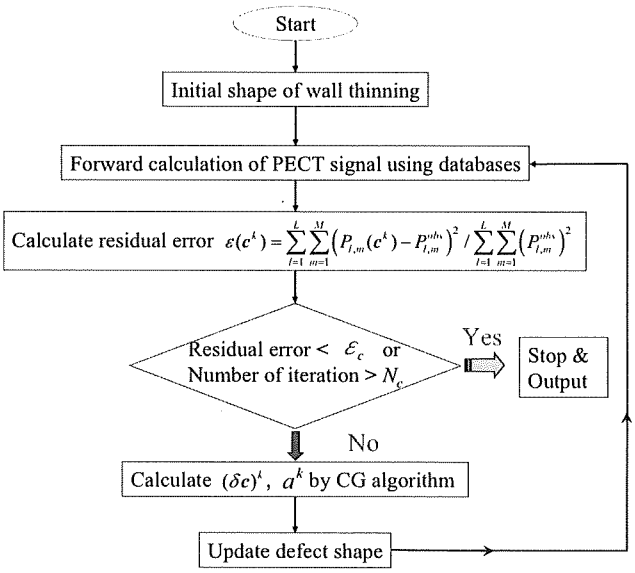

Figure 5. Program flow chart of inverse problem

3.3 Reconstructed examples

The inversion algorithm preceding and the corresponding developed inverse analysis code are validated by 3D wall thinning reconstruction from the simulated PECT signals. A block of austenitic stainless steel 316, with conductivity of 1.35×10^6 S/m, is employed to simulate the big diameter pipe in NPPs as the host conductor, with length 120 mm, width 120 mm, and thickness 10 mm. Wall thinning is located in the bottom side of the specimen. To establish the database for the fast forward solver, the selected possible wall thinning region (search region) is taken as 30 mm in length, 33 mm in width and 10 mm in depth, and subdivided into 550 (10 × 11 × 5) wall thinning cells.

A pancake excitation coil (inner diameter, 5 mm; outer diameter, 10 mm; height, 5 mm; and total number of turns, 296) is applied as the inspection probe. The magnetic flux density in the vertical direction at the position of the bottom center of the excitation coil is selected as the pickup PECT signal. The peak value is extracted from the transient PECT signals as the feature parameter for the wall thinning reconstruction. This is because peak value is more stable in the experimental case (that is, with noisy signals) than the other typical features in PECT signals (peak time, zero crossing time, rising point etc.) [2]. Lift-off is 0.5 mm. A square wave pulse is applied to the excitation coil as the driving current whose DC component is 1.0 A, the period is 0.01s and the duty cycle is 50%. The probe is scanned over the possible wall thinning region part along the length and width direction. Figure 6 shows the schematic of the model.

The computation is carried out on a personal computer, consisting of an Intel (R) Core (TM) i7 CPU 960 @ 3.2 GHz, Memory 6 GB, OS Fedora 12 and Intel Fortran Compiler 10.1.

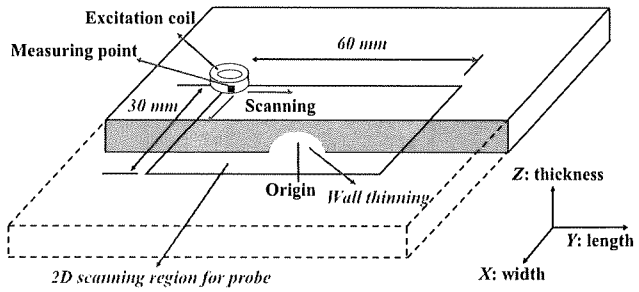

Figure 6. The schematic model for wall thinning detection

According to the wall thinning model introduced in Section 3.1, there are 3 parameters in every row which are: (i) coordinate of left edge of wall thinning in length direction *aw*, (ii) coordinate of right edge of wall thinning in length direction *bw* and (iii) depth *dw*. In our model, the search region is 33 mm in width, subdivided into 11 cells, so the range of w is from 1 to 11. Therefore, originally, there are 33 independent parameters to indicate the shape of 3D wall thinning. However, as general knowledge and our experience with the CG method grows, more parameters will lead to more local minima and the searching difficulty will increase dramatically. However, some artificial restrictions can be applied to the 33 parameters to decrease the degrees of freedom and express a certain 3D wall thinning shape.

In this section, a half ellipse-column wall thinning model is constructed and the reconstruction effect is investigated. Three parameters: *aw*, *bw* and *dw* are used to represent a half ellipse shape in the w-th row, where the half long axis of the ellipse is $(bw-aw)/2$ and the half minor axis of the ellipse is *dw*. Two more parameters of $w1$ and $w2$ ($1\le w1\le w2\le 11$) are added to denote the wall thinning range in the width direction, where the wall thinning in the width direction is from $w1$ to $w2$. And *aw*, *bw*, *dw* do not change when w is within the range $w1$ and $w2$, while *aw*, *bw*, *dw* equal 0 when w is beyond the wall thinning range. Thus a half ellipse-column model of wall thinning with various long axes, and minor axes of half ellipse cross section and width, can be represented using the shape parameter of $\boldsymbol{c}$ = {*aw*, *bw*, *dw*, $w1$, $w2$}.

Figure 7 (a) shows an example of the reconstructed result using the above parameters after 80 iterations, where the shape parameter of true wall thinning is $\boldsymbol{c}$ = {–5.0 mm, 5.0 mm, –50%, 5, 7}; the initial one being {–9.0 mm, 9.0 mm, –30%, 6, 6} and the reconstructed one {–5.008 mm, 5.007 mm, –49.9%, 5, 7}. Figure 7 (b) shows the corresponding peak values extracted from the 2D scanning PECT signal: the true one, the initial one and the reconstructed one. Figure 7 (c) shows the relative residual error. From this, we can see that the size of the wall thinning can be properly reconstructed.

Concerning the time taken, one iteration takes about 3 minutes

and 218 minutes for 80 iterations. From Fig. 7 (c) we find that the residual error decreases rapidly in the first several iterations, with the reconstructed result being {–5.162 mm, 5.161 mm, –49.4%, 5, 7}, and is already quite close to the real one by the 20th iteration.

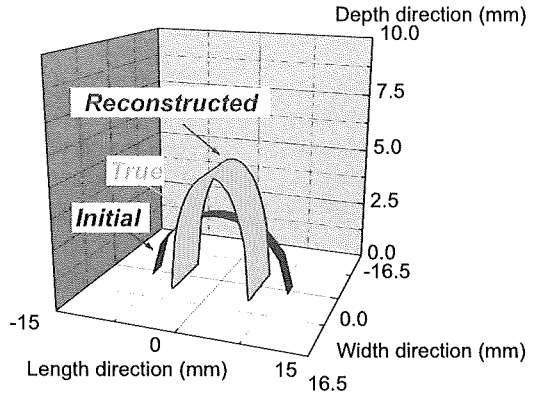

(a) Wall thinning shape: true, initial and reconstructed;

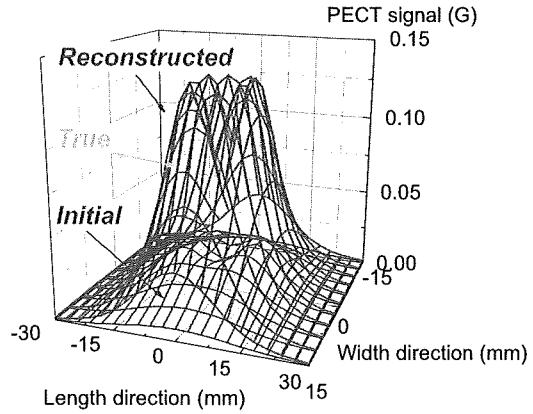

(b) Peak value of PECT signal;

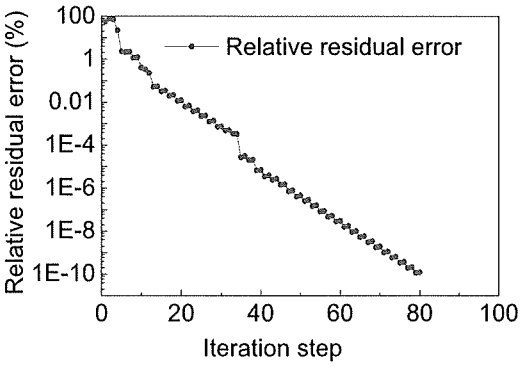

(c) Relative residual error vs iteration step

Figure 7. Reconstructed effect for the half ellipse-column wall thinning model

4 Summary

An efficient and fast numerical solver for simulation of PECT signals has been proposed and developed. Comparison of the numerical results shows that the proposed efficient solver can significantly reduce the simulation time of PECT signals (100 times faster) without losing numerical accuracy. In addition, a PECT inversion algorithm for sizing of 3D wall thinning is proposed based on the developed efficient simulator of PECT signals in present study and a deterministic optimization strategy. Reconstructed results using simulated PECT signals show that the profile of 3D wall thinning with relatively simple shapes can be properly reconstructed using this proposed inversion scheme. Finally, the feasibility of QNDT to wall thinning in stainless steel pipes using PECT method is validated.

Acknowledgments

This work was conducted as a part of Nuclear and Industrial Safety Agency (NISA) project on Enhancement of Ageing Management and Maintenance of Nuclear Power Plants in Japan and supported by the Grant-in-Aid for the Global COE Program, from the Ministry of Education, Culture, Sports, Science and Technology (MEXT) of Japan. The authors would like to thank the National Magnetic Confinement Fusion Program of China (Grant. 2009GB104002), and the Natural Science Foundation of China (Grant Nos. 50977070 and 11021202) for funding this study.

References

[1] K. Takahashi, K. Ando, M. Hisatsune, and K. Hasegawa, Failure behavior of carbon steel pipe with local wall thinning near orifice, *Nuclear Engineering and Design*, Vol. 237, pp. 335-341, 2007.

[2] G. Y. Tian and A. Sophian, Defect classification using a new feature for pulsed eddy current sensors, *NDT & E International*, Vol. 38, pp. 77-82, 2005.

[3] W. Cheng and I. Komura, Simulation of transient eddy-current measurement for the characerization of depth and conductivity of a condutive plate, *IEEE Transactions on Magnetics*, Vol. 44, pp. 3281-3284, 2008.

[4] Z. Chen, K. Aoto, and K. Miya, Reconstruction of cracks with physical closure from signals of eddy current testing, *IEEE Transactions on Magnetics*, Vol. 36, pp. 1018-1022, 2000.

[5] Z. Chen, N. Yusa and K. Miya, Some advances in numerical analysis techniques for quantitative electromagnetic nondestructive evaluation, *Nondestructive Testing and Evaluation*, Vol. 24, pp. 69-102, 2009.

[6] H. Tsuboi, N. Seshima, I. Sebestyén, J. Pávó, S. Gyimothy and A. Gasparics, Transient eddy current analysis of pulsed eddy current testing by finite element method, *IEEE Transactions on Magnetics*, Vol. 40, pp. 1330-1333, 2004.

[7] S. Xie, Z. Chen, T. Takagi and T. Uchimoto, Efficient numerical solver for simulation of pulsed eddy current testing signals, *IEEE Transactions on Magnetics*, Vol. 47, pp. 4582-4591, 2011.

[8] T. Takagi, H. Huang, H. Fukutomi, and J. Tani, Numerical evaluation of correlation between crack size and eddy current testing signal by a very fast simulator, *IEEE Transactions on Magnetics*, Vol. 34, pp. 2581-2584, 1998.

[9] Z. Chen, K. Miya and M. Kurokawa, Rapid prediction of eddy current testing signals by using A-φ method and database, *NDT & E International*, Vol. 32, pp. 29-36, 1999.

[10] S. Xie, Z. Chen, L. Wang, T. Takagi and T. Uchimoto, An inversion scheme for sizing of wall thinning defect from pulsed eddy current testing signals, *International Journal of Applied Electromagnetics and Mechanics* (In press, 2011).

[11] S. J. Norton and J. R. Bowler, Theory of eddy current inversion, *J. Appl. Phys.*, Vol. 73, pp. 501-512, 1993.